Journal of Alloys and Compounds, 213/214 (1994) 159–168
JALCOM 4037

Analysis of recent measurements of the heat capacity of uranium dioxide

C. Ronchi and G.J. Hyland*
Commission of the European Communities, Joint Research Centre, Karlsruhe Establishment, European Institute for Transuranium Elements, Karlsruhe (Germany)

Abstract

Recent measurements of the heat capacity of UO_2 are analysed in the temperature range from room temperature to 8000 K. The high temperature behaviour of $c_p(T)$ is essentially governed by heat energy exchange mechanisms in the solid, involving the formation of atomic and electronic defects. The analysis is centred on the λ transition observed at $T \simeq 0.8T_m$, which is interpreted in terms of the cooperative formation of anion Frenkel defects. Electronic defects, in the form of localized small polarons, formed in the same temperature range, are shown to provide only a minor contribution to c_p, owing to electron–hole interactions. Schottky defects are predicted to play an effective role only between 2700 K and T_m. The decrease in the heat capacity above the melting point of the material is attributed principally to the saturation of the thermally activated contributions. The heat capacity in the liquid is sustained by molecular vibrations up to 4500 K; only at higher temperatures do more energetic electronic excitations take place. The formation of defects in the solid is described by using mean-field models which are able to reproduce the observed transition and its dependence on the stoichiometry in $UO_{2\pm x}$.

1. Introduction

The heat capacity of nuclear oxide fuel is an important quantity in the analysis of severe reactor accidents in which rapid adiabatic core temperature excursions are considered. Although the thermodynamic properties of UO_2 have been carefully measured in the last few decades, solid and liquid measurements above 2500 K are still rare and difficult to interpret. For this reason, within the framework of the Research Safety Programme of the European Communities the high temperature heat capacity of solid and liquid UO_2 has been recently thoroughly investigated in the temperature range 2500–8000 K [1, 2]. The consolidated experimental data now enable a more accurate quantitative analysis to be carried out on the elementary heat exchange mechanisms operating in the different temperature regimes. This paper is a condensed description of a new attempt to provide a simple, unified picture of the high temperature behavior of c_p.

2. Experimental results

Figure 1 shows the complete set of experimental measurements of c_p above room temperature in nominally stoichiometric UO_2. The solid data are obtained by differentiation of enthalpy measurements [3–6] and, in the vicinity of the λ peak, by direct dynamic measurements [2]. The liquid data are taken from ref. 1. The error bars are indicated in different temperature regimes. The measurement accuracy decreases with increasing temperature, as a consequence of the deterioration of the calorimetric and thermal measurements, and of the uncontrolled variation of the chemical composition of the sample. Finally, in the liquid, where

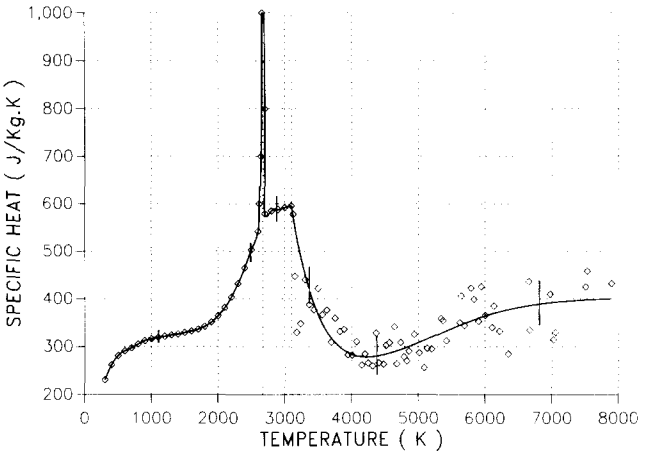

Fig. 1. Heat capacity of nominally stoichiometric UO_2: experimental points and least-squares fitting curve.

*Present address: University of Warwick, Department of Physics, Coventry, UK.

SSDI 0925-8388(94)04037-5

non-smoothed data are plotted, the error mainly results from the particularly difficult experimental method adopted [7]. The full line, which represents a polynomial least-squares fitting of the experimental points, is sufficiently well defined to be used in the analysis of the data.

2.1. Heat exchange stages

The curve $c_p = c_p(T)$ can be qualitatively subdivided into six segments, according to the dominant heat exchange mechanisms operating in the respective temperature intervals.

(1) From room temperature to 1000 K, the increase in heat capacity with temperature is governed by progressive excitation of the harmonic lattice vibrations, which can be approximately described by a single effective Debye model. Since the Debye temperature of UO_2 in this temperature range is less than 600 K, the Debye function is almost unity by $T > 1000$ K, where $c_p^{\text{harm.}}$ attains the Neumann–Kopp asymptotic limit of 9 K, characteristic of a crystal based on a triatomic molecule. A minor contribution is provided by thermal excitation of localized electrons of U^{4+} $(5f)^2$ in the crystal field (CF) levels. At low temperatures, this contribution is approximately proportional to T, while, at high temperatures, where the concentration of U^{4+} decreases by disproportioning into U^{3+} and U^{5+}, c_p^{CF} becomes essentially temperature independent.

(2) From 1000 to 1500 K, c_p continues to increase weakly with T, as a result of the progressive increase in the anharmonicity of the lattice vibrations, as reflected in the thermal expansion of the material. The slope of $c_p(T)$ resulting from these effects, measured in different compounds with similar mechanical properties, reveals an almost constant trend which can be used to extrapolate $c_p^{\text{anharm.}}$ to higher temperatures.

(3) From 1500 to 2670 K ($= T_t$), the additional increase in c_p is caused by the formation of lattice and electronic defects. The c_p peak measured at approximately $T = 0.8T_m$ (which indicates a sharp thermodynamic transition) is very similar to that observed in other ionic fluorides which exhibit a superionic λ transition. Following ref. 8, this transition is interpreted as a cooperative process involving the creation of defects in the sublattice of the more mobile atomic species, leading to a sudden increase in the oxygen Frenkel pair concentration at a defined critical temperature T_t [5]. This assumption was later corroborated by neutron scattering measurements of the oxygen defect concentration n_F as a function of the temperature [9], which showed a steep inflection point at $T = T_t$. Moreover, the d.c. electrical conductivity of UO_2 is known to increase sharply in this temperature interval [10], entailing a further contribution to the heat capacity.

(4) From T_t to T_m, c_p is characterized by a steep descending flank of the transition peak, as a result of the rapid saturation of the defect concentration (anion-disordered phase), followed by a weakly increasing stage resulting from the onset of the creation of more energetic atomic defects (UO_2 Schottky trios).

(5) From T_m to 4500 K, the heat capacity decreases to the level attained at 1000 K, indicating that all the thermally activated processes have completely saturated, leaving only atomic vibrations to support further heat exchanges.

(6) From 4500 to 8000 K, an upswing in c_p is observed, with an activation energy comparable with that needed in the solid to excite the electrons of the deeper 2p-based valence band.

From this brief overview of the elementary mechanisms contributing to the heat capacity of UO_2, one realizes that the central problem for a comprehensive microscopic model of the system is a description of the atomic and electronic defect behaviour described in points (3) and (4). In fact, in this temperature range, other relevant thermodynamic and thermophysical properties (defect concentrations, electrical and thermal conductivity [11], creep rate [12] and, probably, self-diffusion coefficient [13]) present "anomalies" which should be encompassed and explained by realistic models.

2.2. Properties of the λ transition in UO_2

For a long time, the results concerning the λ transition in UO_2, obtained by differentiating the enthalpy H, have been very controversial – even the existence of the transition was initially questioned by some authors, who interpreted the c_p peak obtained by finite-difference calculation of dH/dT (even that using a more sophisticated numerical analysis [14]) as an experimental artifact. Only more recent experiments specifically aimed at detecting this effect [2] could provide unambiguous and more detailed evidence. By using a thermo-analytical method based on the cooling curve analysis of a laser-pulse-heated sample, a premelting transition was observed in the form of a marked minimum in the cooling rate dT/dt. Since, under fixed heat loss conditions, dT/dt is inversely proportional to c_p, the c_p transition peak could be reproduced with good accuracy by using an appropriate numerical analysis. Figure 2 shows the results obtained in a nominally stoichiometric sample.

The transition appears at 2670 K and the resulting heat capacity peak (Fig. 3) – over the assumed "unperturbed" c_p background – is high and very narrow*. This explains the difficulty in detecting the transition by performing numerical differentiation of H. The experiments have been repeated under both reducing and

*The calculation of the peak was made by assuming a smoothed $c_p(T)$ curve, without a peak, such as would have been entailed by a cooling curve with no inflection points.

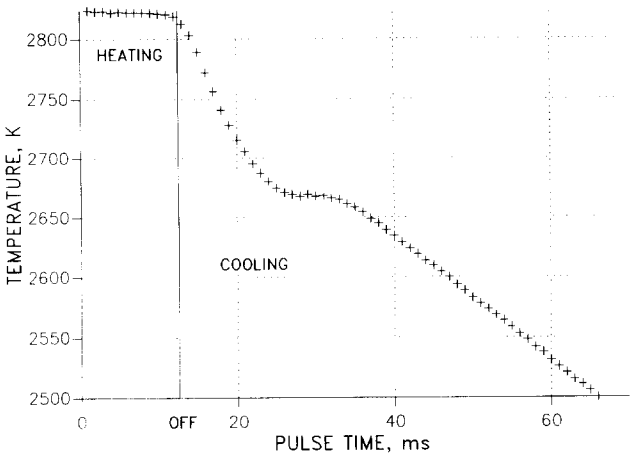

Fig. 2. Cooling curve of a UO_2 sphere of diameter 1 mm, showing a λ transition at 2670 K, in the form of a strong decrease in the cooling rate. The sample was laser heated up to the pulse time indicated by "OFF".

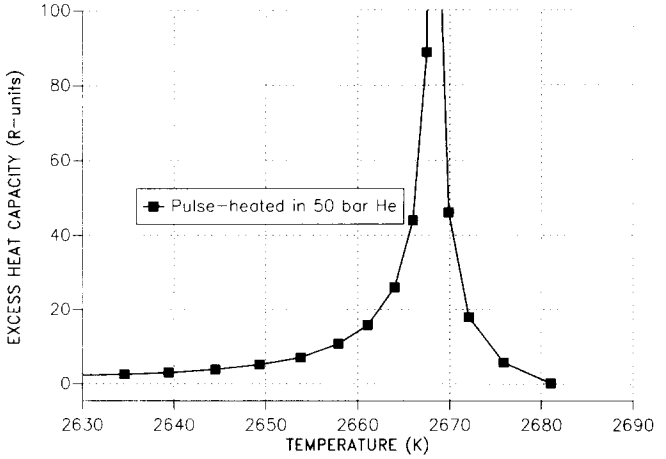

Fig. 3. Heat capacity peak resulting from the λ transition, from the data in Fig. 2.

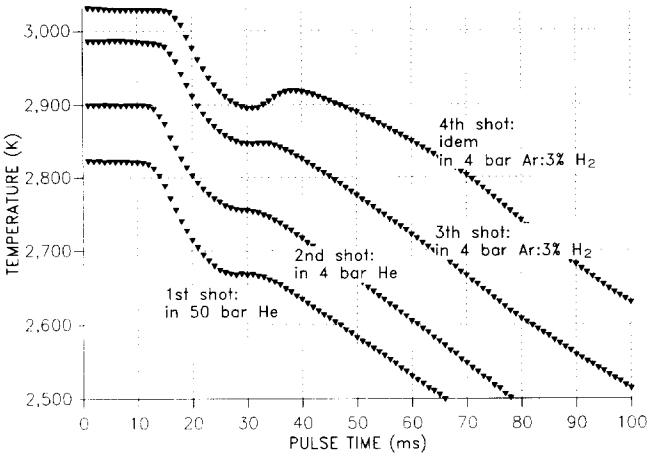

Fig. 4. Cooling curves from a sequence of pulses on a UO_2 sample under reducing conditions, showing the increase in the transition temperature with decreasing sample stoichiometry.

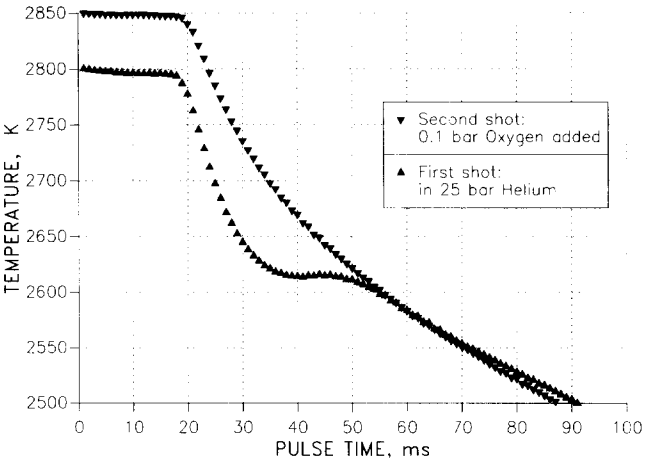

Fig. 5. Cooling curves of a UO_2 sample under inert and oxidizing conditions, showing the disappearance of the transition in UO_{2+x}.

oxidizing atmospheres, and the following interesting results obtained.

(1) For O/U < 2, the transition temperature increases with increasing reduction. Moreover, in reduced samples, supercooling effects are observed, involving an inversion in the sign of dT/dt. This provides a clear indication that the transition producing the cooling rate perturbation was of first order (Fig. 4)*.

(2) Under oxidizing conditions (O/U > 2), no inflection points are detected during cooling (Fig. 5), and it appears that there is no transition of the kind found in stoichiometric and substoichiometric UO_2.

*This effect is well known. For instance, during rapid cooling from the liquid, the temperature can decrease below the freezing point, whereby the sample remains in a glassy form, without releasing the latent heat of fusion. This continues until, after a finite time, the crystal phase is nucleated. The ensuing crystallization process, driven by a $\Delta\tilde{S} < \Delta S_f$, may lead to the formation of anomalous metallographic features.

3. Points defects in UO_2

In this section, microscopic models for lattice and electronic defect formation are examined, with the intention of explaining the high temperature behaviour of c_p in UO_2. This is in the context of the experimental evidence already mentioned (*i.e.* magnitude of $c_p(T)$, position and nature of the premelting transition, and its dependence on stoichiometry, together with equilibrium defect concentration as a function of temperature). Three types of defect are considered here: (a) oxygen Frenkel pairs, (b) neutral trios of Schottky vacancies and (c) a valence alteration of the lattice cations. Their respective formation reactions are written as

$$O_L^{2-} + V_I^0 \longrightarrow V_L^0 + O_I^{2-} \quad (1)$$

$$U_L^{4+} + 2O_L^{2-} \longrightarrow V_L^U + 2V_L^0 \quad (2)$$

$$2U^{4+} \longrightarrow U^{3+} + U^{5+} \quad (3)$$

where the symbols are self-explanatory.

Once the free energies of formation of the three reactions are given, the corresponding law of mass action equations, together with three additional constraint equations dictated by charge neutrality, chemical composition and structural configuration of the fluorite crystal unit cell, are sufficient to define the equilibrium concentrations of the defects involved. However, a few remarks concerning the relationship between the formation of these defects in UO_2 and the observed λ transition are in order.

(1) The λ transitions occur in the vicinity of 2650 K in both stoichiometric and nearly stoichiometric UO_2, and primarily result from cooperative (anti-)Frenkel anion disorder, whose associated free energy of formation is much lower than that of the Schottky trio disorder (see, for example, refs. 15 and 16) to which the Frenkel disorder is coupled (in the law of mass action) via the equilibrium oxygen vacancy concentration. In turn, the Schottky defect concentration is dependent on the disproportionation fraction of U^{4+} (see below). Near the stoichiometric O/U ratio, this fraction is close to unity, even at high temperatures, so the ionic disorder can be decoupled from the electronic disorder. Furthermore, since the Schottky trio formation energy is nearly twice that of an oxygen Frenkel pair, the two types of defect are effectively formed and reach saturation in different temperature intervals. Therefore, in a first approximation, Frenkel disorder can be solved independently of the Schottky disorder.

(2) Assuming that the bonding in UO_2 is principally ionic, the cations in the stoichiometric material are nominally U^{4+} $(5f)^2$. The possibility of relatively low energy fluctuations about this configuration (to U^{5+} and U^{3+}) then permits the following: (a) the accommodation within the fluorite phase of a large degree of non-stoichiometry – in the hyperstoichiometric case, the excess oxygen is assumed to occupy interstitial sites, with the formation of neutralizing U^{5+} ions, while the hypostoichiometric case is characterized by oxygen vacancies and U^{3+} ions; (b) intrinsic electronic semiconductivity [10] in stoichiometric UO_2 originating from the thermally induced cation disproportionation $2U^{4+} \rightarrow U^{3+} + U^{5+}$ [17–19] – in this context, it is worth remarking that, near the c_p peak temperature T_t, the d.c. electrical conductivity is approximately one order of magnitude higher than that which characterizes purely ionic conductors, even in their fast ion phase.

(3) Owing to the strong interaction with the polar lattice, the supranumerary electrons and holes associated, respectively, with the U^{3+} and U^{5+} ions (formed either by reaction (3) or by stoichiometry deviation) are localized in small polaron eigenstates. In these states, electrons and holes are associated with local atomic relaxations in the polar lattice, and carrier motion takes place by 'hopping", the associated mobilities then being activated, as in the case of atomic defects. Although, from a formal point of view, this permits a common treatment, it can give rise to difficulties when it comes to distinguishing the respective contributions to c_p. This point will be returned to in section 5.

(4) UO_2 exhibits a significant increase in creep rate above T_t, *i.e.* much more than is expected from extrapolation of lower temperature data. The plasticity above 2700 K is so high that a high density sintered UO_2 sample annealed above this temperature for a few hours is subject to large permanent deformations, even in the absence of external applied stresses*. The effect is confirmed by a decrease in the rigidity modulus [21], which is much stronger than that observed in the case of fluorides undergoing superionic transition [22]. Thus, it is evident that the λ transition in UO_2 indicates the onset of potentially significant changes in the structural stability of the material.

4. Microscopic models for the λ transition

The mean-field models presented in this section attempt to lay the foundations of an understanding of the behaviour of the heat capacity between 1500 K and the melting point, simply by describing the temperature dependence of the equilibrium concentration of the above-mentioned point defects. Owing to the limitations of space, only the salient aspects of the analysis are discussed here; more details concerning new developments will be published in a separate paper.

4.1. Linear model for cooperative Frenkel defect formation

The simplest model capable of describing the effects associated with the cooperative defect formation in a system is based on the assumption that the free energy of formation of one additional defect decreases linearly with the concentration n of the pre-existing defects. The free energy of formation, referred to the free energy of the perfect crystal, is then

$$\Delta G = [O_I]\left\{\Delta H_0 - \frac{\lambda}{2}[V_L^0] - kT(\Delta S^c + \Delta S^{nc})\right\} \quad (4a)$$

for UO_{2-x} and

$$\Delta G = [V_L^0]\left\{\Delta H_0 - \frac{\lambda}{2}[O_I] - kT(\Delta S^c + \Delta S^{nc})\right\} \quad (4b)$$

*Even the ceramographic grain boundary structure appears to be rounded – similar to that observed by cooling after melting. The effect is sometimes so striking that early experimenters were induced into the error of taking 2700 K as the melting temperature [20].

for UO_{2+x}, where the superscripts c and nc stand for "configurational" and "non-configurational" respectively. ΔH_0 is the enthalpy of formation in the absence of interaction. λ represents a mean attractive energy between complementary defects (oxygen interstitials and vacancies); for an isotropic and homogeneous distribution of defects, this produces a lowering of the formation energy below the defect-free value ΔH_0. It must be stressed that λ is a purely phenomenological model parameter, which is not necessarily associated with any physically definable interaction configuration (but may, under certain conditions, be identified with the first term of a series expansion of such).

In eqn. (4), the configurational formation entropy ΔS^c for a Frenkel pair in $UO_{2\pm x}$ takes the form

$$\Delta S^c = k \ln \frac{n(n \mp x)}{(2\beta \pm x - n)(\alpha - n)} \tag{5}$$

where $n \equiv [V_L^0]([O_I])$ for $UO_{2+x}(UO_{2-x})$, *i.e.* it corresponds to the pertinent intrinsic defect concentration, β is the effective fraction of oxygen lattice sites per unit cell available for occupation by V_L^0, and α is that of interstitial sites for occupation by O_I. α and β are less than unity, since the repulsive interaction between like defects tends to discourage (*i.e.* "blocks") the occupancy of neighbouring sites [23]*. Consideration of the crystallographic configuration of the lattice relaxations around a defect [24] suggests that interstitial and vacancy site blocking should be extended to the nearest and next-nearest neighbour sites, respectively, so that one can write

$$\alpha = (1 + 12[O_I])^{-1}$$
$$\beta = (1 + 18[V_L^0])^{-1} \tag{6}$$

where both $[O_I]$ and $[V_L^0]$ may be expressed in terms of the relevant intrinsic fractional concentration n of defects and stoichiometry deviation, x. Therefore $\partial \Delta G / \partial n$ is a function of n and of five additional parameters (T, x, ΔH_0, λ, ΔS^{nc}).

Thermodynamic equilibrium at a given T requires that n satisfies the equation

$$\frac{\partial \Delta G}{\partial n} = 0 \tag{7}$$

Now, for a given x, the solution $n(T)$ of eqn. (7) in the space of the model parameters ΔH_0, λ and ΔS^{nc} can be either a monotonic continuous function, increasing from zero up to a positive asymptotic value, or a function displaying a discontinuity at a distinct temperature $T = T_t$, *i.e.* a first-order phase transition between a low-temperature ordered phase and a high-temperature disordered phase. The two types of solution are separated by an interface, where the discontinuity step of $n(T)$ at $T = T_t$ is reduced to a continuous segment with a vertical inflection point. This occurs when, in addition to eqn. (7), the following conditions hold:

$$\frac{\partial^2 \Delta G}{\partial n^2} = 0, \qquad \frac{\partial^3 \Delta G}{\partial n^3} = 0 \qquad \frac{\partial^4 \Delta G}{\partial n^4} > 0 \tag{8}$$

Systems satisfying these conditions undergo a phase transition of the second order; formally, this transition is analogous to that occurring at a thermodynamic critical point. Equations (8) reduce the free parameters of the model (λ, ΔH_0 and ΔS^{nc}) from three to one. Furthermore, for a given configurational defect formation entropy, and for a constant ΔS^{nc}, the second-order critical value λ_{crit} is independent of the other two parameters. The occurrence of a second-order transition in nature may appear as occasional and rather improbable. However, a more in depth view of the argument leads to a different conclusion. In fact, an increase in λ from zero to values above λ_{crit} produces a passage from a diffuse to a first-order transition, through a sequence of transitions which differ very little from each other. In contrast, we expect that, in a cooperative system, λ depends both on the nature of the defects themselves and on their arrangement (mutual orientation, clustering, short-range order and, in the limit, defect long-range order), *i.e.* it arises from the structural context with which the defect is merged. Now, in a system for which eqns. (8) satisfied the free energy is fairly insensitive to the local defect concentration (the first non-zero derivative is the fourth). The argument can be reversed, by inferring that, in a complex system, where strongly interacting defects are allowed to assume a variety of local configurations (as, for instance, in the case of fluorite structures), a second-order critical point is likely to be found.

Therefore, it was assumed that, in stoichiometric UO_2, the λ transition was produced by Frenkel defect formation, described by eqn. (4), and that the interaction parameter and the non-configurational defect formation entropy satisfy eqns. (8) at $T = 2670$ K. Thus, the only input parameter was ΔH_0, the value of which

$$\Delta H_0 = 3.67 \text{ eV} \tag{9}$$

was taken from neutron scattering data [9]. The solution of eqn. (8) then yields the following critical values for the model parameters:

$$\lambda_{crit} = 2.74 \text{ eV} \quad \Delta S^{nc}_{crit} = 12.8\, k \quad n_{crit} = 0.13 \tag{10}$$

The case of $UO_{2\pm x}$ was then considered, under the following hypotheses:

*Alternatively, the formation of defect clusters which engage more than one lattice site can be considered; again, this can be described by using a "site blocking" formalism.

(1) the value of the defect interaction parameter remains unchanged;

(2) the non-configurational entropy ΔS^{nc} varies linearly with the equilibrium defect concentration.

The first assumption can entail the non-existence of a second-order transition in non-stoichiometric compounds, while any other type of transition that may occur may be located at $T \neq 2670$ K. The second hypothesis enables us to reproduce the experimental finding concerning the nature of the transition in the hypostoichiometric case, *i.e.* the appearance of first-order transitions at progressively higher temperatures. With these assumptions, one finds

$$\Delta S^{nc} = 9.5(1+3n)k \qquad (11)$$

These parameters have been used to calculate the behavior of the material in the stoichiometry range $1.85 < O/U < 2.25$. The curves of the resulting $c_p = c_p(T)$ and $n = n(T)$ values are plotted in Figs. 6 and 7. The results are summarized in Fig. 8, where the second-order critical parameters are plotted as functions of x and are compared with the assumed non-configurational entropy of eqn. (11), whose magnitude with respect to its critical value defines the nature of the expected transition: for $\Delta S^{nc} > \Delta S^{nc}_{crit}$, the transition is of first order; for $\Delta S^{nc} < \Delta S^{nc}_{crit}$, the transition is of diffuse type, with a finite c_p peak height.

Starting from UO_2, where the premelting transition is of the second order, the model predicts for hypostoichiometric oxides a first-order transition, with the transition temperatures increasing with x. The maximum transition temperatures $T_t = 2870$ K is calculated for $x \simeq -0.1$ At higher oxygen deficiencies, the transition becomes — as one would obviously expect — of the diffuse type, with the defect concentration increasing

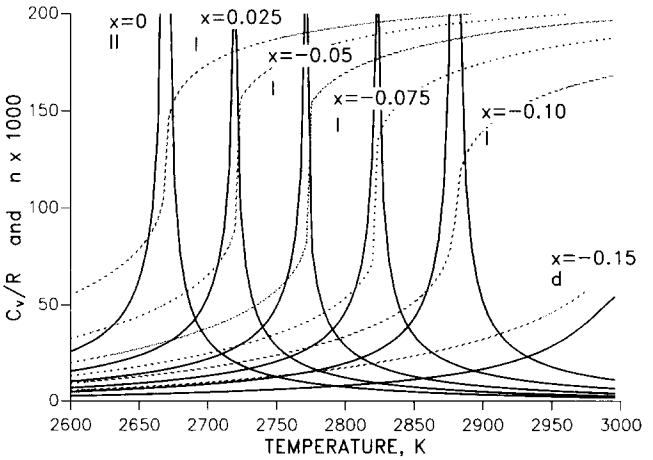

Fig. 6. Calculated heat capacity contribution (——) from Frenkel disorder and defect equilibrium concentration (· · · · ·) as functions of T in UO_{2-x} at various values of x. For $x < 0$, c_p diverges at the peak temperature, where a first-order transition is predicted. The concentration $n(T)$ is discontinous at the peak position.

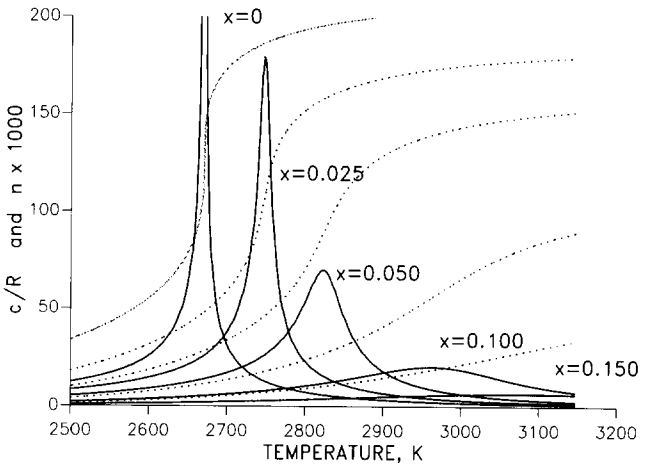

Fig. 7. Calculated heat capacity contribution (——) from Frenkel disorder and defect equilibrium concentration (· · · ·) as functions of T in UO_{2+x} at various values of x. For $x > 0$, c_p is large, but finite, at the peak temperature, where a "diffuse" transition is predicted. The concentration $n(T)$ has a non-vertical inflection at the peak position.

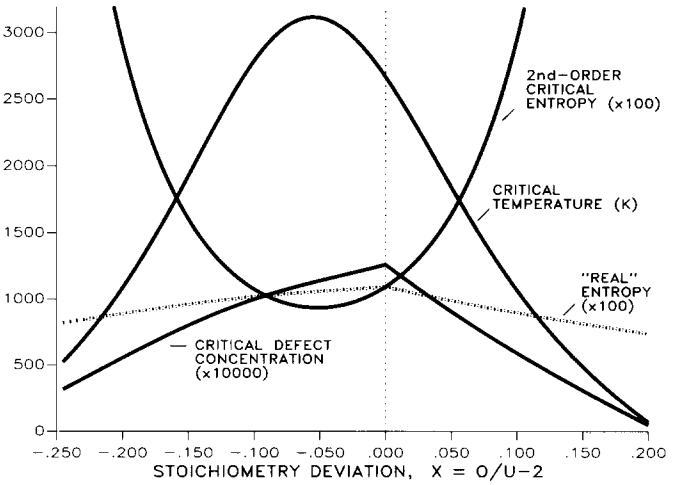

Fig. 8. Critical parameters for a second-order transition in $UO_{2\pm x}$. The position of the actual non-configurational entropy below or above its critical value entails a "diffuse" or first-order transition respectively.

continuously with temperature. This trend is in agreement with the results of the experiments performed under reducing conditions (Fig. 4). In the hyperstoichiometric oxide, a diffuse transition is predicted, with the peak height decreasing with x. This entails that the transition becomes progressively less pronounced and, at a sufficiently high value of x, it effectively disappears, which is in agreement with the experimental findings. Unfortunately, the O/U analysis of the oxidized samples (Fig. 5) could not be performed; estimates from extrapolated oxygen potentials indicate that $O/U > 2.1$. If one compares this value with the curves in Fig. 5, one can see that, at these stoichiometries, the predicted transition is of diffuse type and very broad, with the

heat capacity peak positioned at temperatures above the melting point. (Only conjectural data are available on the decrease in the melting point in highly hyperstoichiometric UO_{2+x}.)

4.2. Comparison with the classical Debye–Hückel model

The results of the phenomenological linear model can be compared with the predictions of a statistical mechanical model based on a physically well-defined interaction – the Coulomb interaction. To this end, we have chosen the original Hückel model, because it is perfectly self-consistent within the legitimacy limits of the Debye approximation of Boltzmann's formula. We recall that the Hückel model is based on the assumption that the defects interact in an isotropic electric polarization field described by a macroscopic static dielectric constant; the defects are assumed to be rigid spheres, with the closest distance of approach.

The defect interaction energy, corresponding to the second term on the right-hand side of eqn. (4) now takes the form [25]

$$\Delta G^{el} = \frac{n|ze|^2\kappa}{3D}\,\tau(\kappa a) \tag{12}$$

where D is the static dielectric constant, ze is the defect charge and κ is the inverse Debye screening length, defined by

$$\kappa^2 = \frac{4\pi n|ze|^2}{VDkT} \tag{13}$$

where V is the molecular volume and $\tau(y)$ is a function arising from the integration of the electrostatic potential, such that

$$\tau(y) = \frac{3}{y^3}\left\{\log(1+y) - y + \frac{1}{2y^2}\right\} \tag{14}$$

Equations (13) and (14) were then used to replace in eqn. (4) the interaction term proportional to λ; the second-order transition parameters were then searched for by solving eqns. (7) and (8). In contrast to the linear model, this system of equations only has real solutions for $\Delta H_0 > 4.6$ eV; while this value is larger than that used in the linear model (3.6 eV), it still falls within the experimental range. Figure 9 shows that, at the critical temperature, the linear model and the Hückel model predict a similar behavior of $c_p(T)$ and $n(T)$. Knowing the critical parameters κ_{crit} and n_{crit}, we can solve eqn. (13) for the effective dielectric constant, to give

$$D = 19.8 \tag{15}$$

which falls in the range of the experimental values ($20 < D_{exp} < 24$). This result is particularly important in connection with the effects described in the following section.

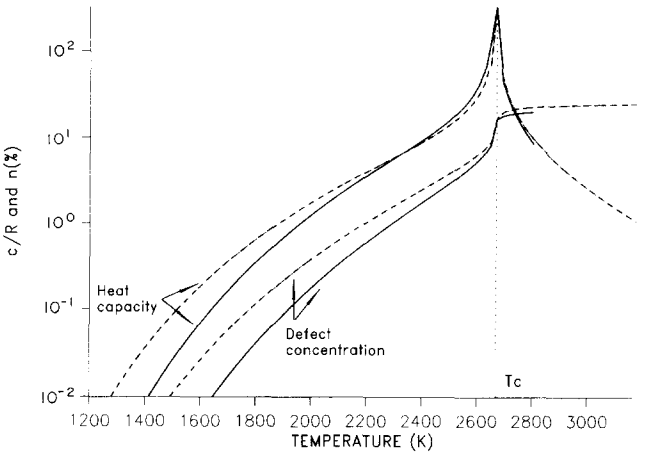

Fig. 9. Comparison of the Frenkel defect concentration and heat capacity contribution calculated by using the linear interaction (——) and the classical Debye–Hückel model (– – –).

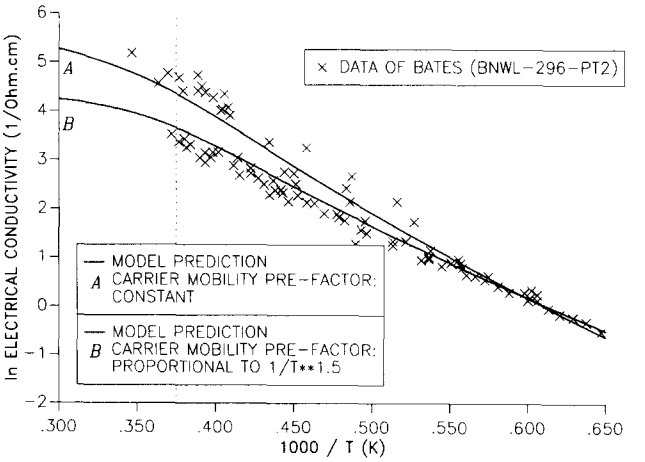

Fig. 10. D.c. electrical conductivity measurements and theoretical predictions (×) from the interacting polaron model (——). The two lines A and B correspond to two different carrier mobility rules.

5. Small polaron contribution

The small polaron c_p contribution associated with the defect equilibrium concentrations predicted by reaction (3) takes the form of a thermally activated process. The experimental basis for the evaluation of the relevant parameters is provided by the d.c. electrical conductivity data, *i.e.* $\sigma = \sigma(T)$, plotted in Fig. 10. Customarily, in the analysis of these data, the increase in $\sigma(T)$ is interpreted as a single-energy activated process, where the carrier concentration is approximated by an exponential function of T^{-1}, and their hopping mobility involves a prefactor proportional to $T^{-1.5}$. From this treatment, the contribution of small polarons to the

heat capacity turns out to be far too large to be in any way compatible with the coexisting contribution from oxygen defects. This problem is reflected by the conclusions of earlier papers, where the upswing in c_p at high temperatures was attributed either to atomic (see, for example, ref. 26) or to electronic defects (see, for example, ref. 27). However, inspection of the conductivity data at high temperatures indicates a significant deviation from a simple exponential dependence of the carrier concentration on T^{-1}, which we have interpreted as evidence for cooperative small polaron formation. Therefore, we followed Yoffa and Adler [28], who used a Hückel-type model to describe the temperature-induced transition to the metallic state in Mott insulators.

5.1. *Quantum mechanical cooperative model for small polaron formation*

In this model [28], based on the Hubbard Hamiltonian, the on-site Coulomb repulsion U between like defects (the U^{3+} and U^{5+} small polarons) takes the form

$$U = U_0 \exp\left\{ -\left(\frac{8\pi e^2 a^2 n}{kTVD} \right)^{1/2} \right\} \tag{16}$$

where the symbols are the same as in eqn. (12). U_0 (the bare intrasite Coulomb repulsion or Hubbard gap) is essentially analogous to the perfect crystal Frenkel formation energy ΔH_0 defined above. It should be noted that $\hat{n}$ represents the *equilibrium* concentration of defects and *not a free variable*. (In their model, Yoffa and Adler faced the well-known self-consistency problem and had to introduce this additional "Ansatz". In fact, all the "improved" Hückel solutions are generally not self-consistent (for example, ref. 29). For the problem of conforming the statistical mechanics scheme of assemblies with temperature-dependent energy levels to the demands of thermodynamics, see ref. 30.)

The model was applied to describe small polaron formation in the presence of electron–hole interactions. U_0 was calculated from the Arrhenius regime of the intrinsic conductivity data to be 2.34 eV, while the exponent in eqn. (16) was adjusted to obtain the best fit of the experimental $\sigma(T)$ data. As in the preceding models, the effect of the screening was to inflect the curve $n = n(T)$ in a narrow temperature range. For a sufficiently high screening constant and defect concentration, the Hubbard gap collapses and the first-order transition from an insulating to a metallic state occurs. Since this transition is not observed in UO_2, the range of variation of the screening constant was relatively small, and the fitting procedure fairly unambiguous. The results are plotted in Fig. 10 as full lines.

The effective dielectric constant was finally evaluated from the screening constant as:

$$D = 18 \pm 1 \tag{15}$$

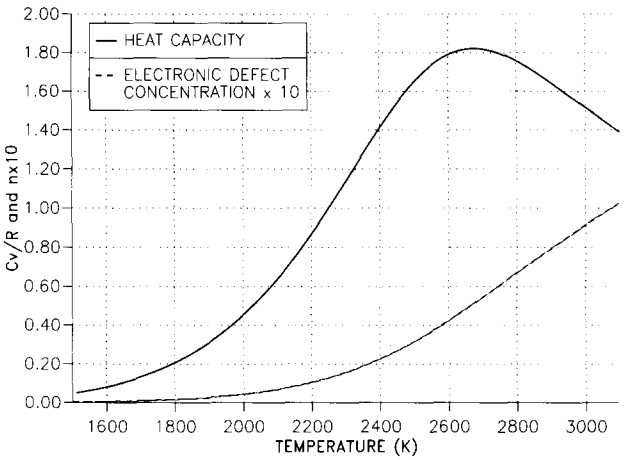

Fig. 11. Model prediction of the small polaron concentration and heat capacity contribution.

which again is in fairly good agreement with the value calculated – in the quite different defect context of the oxygen Frenkel pair formation – and, of course, with experimental findings.

The important consequence of including polaron–polaron interactions is that the resulting heat capacity contribution is sufficiently reduced (Fig. 11) to be able to be accommodated in the total balance of the other c_p contributions.

6. Schottky disorder

The simplest variety of cation disorder most likely involves the formation of a trio of vacancies, according to reaction (2). It should be noticed that V_L^0 already occurs in the Frenkel disorder discussed above; thus, the two disordering processes are coupled. However, given the much higher value of the formation energy of Schottky defects (ΔH_0^S), their effect on the Frenkel disorder can be practically neglected, as was implicitly done above in our treatment of the λ transition; the opposite does not hold, however.

While the reliability of the value (about 6.5 eV) currently assigned to ΔH_0^S is difficult to assess, it is of interest to note that this value does satisfy the empirical relationship which holds between ΔH_0^S and T_m of many binary ionic crystals [31]. Therefore, a mean field model of the melting transition, based on cooperative Schottky defect formation, is currently under investigation. In this model, the coupling to the existing Frenkel defects (via the common V_L^0 species) is included. This is because, in the 450 K interval between the λ transition and melting, the degree of anion disorder is appreciable, attaining values of around 20% in $UO_{2.0}$. However, pilot calculations neglecting this coupling indicate a small c_p contribution prior to

TABLE 1. Theoretical contributions to heat capacity and experimental measurements in UO_{2-x} (J mol^{-1} K^{-1})

Temperature (K)	1 Harm.	2 Anh.	3 C.F.	4 Frenkel $x=0$	4 Frenkel $x=0.02$	5 S.P.	6 Schottky	1 to 6 summed $x=0$	1 to 6 summed $x=0.02$	Expt.
1000	74.8	2.5	6.0	0.0	–	–	–	83.3	83.3	84.0
1200	74.8	4.8	6.0	0.0	–	0.1	–	85.7	85.7	86.0
1400	74.8	6.9	6.0	0.3	0.0	0.2	–	88.2	87.9	88.0
1600	74.8	8.9	6.0	1.5	0.0	0.7	–	91.8	90.4	90.0
1800	74.8	10.9	6.0	5.1	0.4	1.7	–	98.5	93.8	93.0
2000	74.8	12.9	6.0	13.7	2.6	3.8	–	111.2	100.1	99.0
2200	74.8	14.8	6.0	34.2	13.6	7.1	–	136.9	116.3	109.0
2400	74.8	16.8	6.0	75.2	44.1	11.7	0.8	185.3	154.2	119.0
2600	74.8	18.8	7.0	264.4	132.4	14.8	1.2	381.0	249.1	200.0
2670	74.8	19.5	7.0	–	–	14.9	1.6	–	–	–
2800	74.8	20.8	7.0	80.9	92.4	14.5	2.2	200.3	211.8	150.0
3000	74.8	22.8	7.0	21.2	20.0	12.6	3.6	142.0	140.7	155.0
3100	74.8	23.8	7.0	13.4	12.5	11.5	4.4	134.9	134.0	161.0

the first-order melting transition at approximately 3120 K. Therefore, the contributions from Schottky disorder included in the synthesis of the following section are only preliminary measures.

7. Synthesis of identified c_p contributions

Calculations of the c_p contributions from the six sources identified and discussed above are presented in Table 1 for the case of stoichiometric UO_2, over the temperature range $1000 < T < T_m$. Comparison of the sum of these contributions with the experimental values, given in the final column, reveals that, while the agreement is good up to 2000 K, the values calculated at higher temperatures are apparently in excess. The agreement is significantly better if the theoretical results for a slightly substoichiometric compound are taken, though the calculated transition peak is still broader than that deduced from the experiment. This invites the following comments on the limits of the adopted model.

We would hardly expect better quantitative agreement with the λ transition than is afforded by the adopted "mean field" model. This has the great merit of correctly reproducing the nature of the transition and its x dependence. Since it involves only a few parameters, it affords a reasonably simple description; however, this may be inadequate in a more precise quantitative context. Two possible causes of discrepancy can be advanced.

(1) One possible cause is our treatment of the different contributions as though they were strictly independent. We have already mentioned that this is particularly unrealistic in the case of the Schottky and Frenkel disorder. Now, the small polaron and Frenkel defect contributions are not independent either. In fact, it should be appreciated that the polaronic nature of the supranumerary electrons and holes necessarily entails an attendant degree of lattice disorder (polarization field strains), involving, in particular, displacement of oxygen ions to relaxed (interstitial) positions. Although the (unknown) actual positions of these atoms may differ from those of the Frenkel interstitials, an interdependence between polaron and Frenkel pair formation appears to be very likely. (An association between a polaron and a Frenkel pair is also strongly suggested by the structure of the simplest 1:2:2 cluster, whose local crystallographic configuration of uranium and oxygen approaches that found in U_3O_8.) Neglecting this effect leads to an overestimate of the c_p contributions of the two kinds of defect.

(2) Another possible cause is the assumed formulation of the attractive part of the internal energy. It is well known that the validity of the mean field approaches based on Debye's approximation is limited to highly dilute systems. At the calculated defect concentrations near the transition (n of the order of 0.1), the validity of the approximation is uncertain. Therefore, from a purely phenomenological point of view, terms involving higher powers of n should perhaps be included, although this would introduce additional empirical parameters. In the absence of more detailed physical hypotheses on the nature of the defect interactions, however, such a model would be of limited theoretical interest.

References

1 C. Ronchi, J.P. Hiernaut, R. Selfslag and G.J. Hyland, *Nucl. Sci. Eng., 113* (1993) 1.

2 J.P. Hiernaut, G.J. Hyland and C. Ronchi, *Int. J. Thermophys., 14*(2) (1993) 259.
3 R.A. Hein and P.N. Flagella, *US Rep. GEMP-578*, General Electric Company, Cincinnati, OH, 1968.
4 J.K. Fink, M.G. Chasanov and L. Leibowitz, *US Rep. ANL-CEN-RSD 80/3 USA*, Argonne National Laboratory, Argonne, IL, 1980.
5 P. Browning, G.J. Hyland and J. Ralph, *High Temp. High Pressure, 15* (1983) 169–178.
6 G.J. Hyland and R.W. Ohse, *J. Nucl. Mater., 140* (1986) 149.
7 J.P. Hiernaut and C. Ronchi, *High Temp. High Pressure, 21* (1989) 119.
8 M.A. Bredig, *US Rep. 4437*, Oak Ridge National Laboratory, Oak Ridge, TN, 1969, p. 103.
9 M.T. Hutchings, *J. Chem. Soc. Faraday Trans. II, 83* (1987) 1083.
10 J.L. Bates, C.A. Hinnan and T. Kawada, *J. Am. Ceram. Soc., 50* (1967) 652.
11 G.J. Hyland, *J. Nucl. Mater., 113* (1983) 125.
12 O.D. Slagle, *J. Am. Ceram. Soc., 67* (1984) 169–174.
13 E.H. Ranklev and C.A. Hinman, *Proc. Int. Conf. on 'Fast Breeder Reactor Fuel Performance', Monterey, CA, March 5–8, 1979*, p. 405.
14 J. Ralph and G.J. Hyland, *J. Nucl. Mater., 132* (1985) 76.
15 H. Matzke, *Adv. Ceram., 17* (1986) 1–54.
16 R.A. Jackson *et al., Philos. Mag. A, 53* (1985) 27.
17 G.J. Hyland and J. Ralph, *High Temp. High Pressure, 15* (1983) 179–190.
18 C.R.A. Catlow, *Proc. R. Soc. London Ser. A, 353* (1977) 533.
19 D.A. McInnes, *Proc. Int. Symp. on Thermodynamics of Nuclear Materials, Jülich, January 29–February 2, 1970,* Vol. 1, IAEA, Vienna, 1980, p. 129.
20 R.J. Ackermann, *US Rep. ANL-5482*, Argonne, National Laboratory, Argonne, IL, 1955.
21 V.M. Carr, A.V. Chadwick and R. Saghafian, *J. Phys. C, 11* (1978) L637.
22 C.R.A. Catlow, J.D. Comins, F.A. Germano, R.T. Harley and W. Hayes, *J. Phys. C, 11* (1978) 3197.
23 K. Hagemark and M. Broli, *J. Nucl. Inorg. Chem., 28* (1966) 2837.
24 B.T.M. Willis, *J. Chem. Soc. Faraday Trans. II, 83* (1987) 1073.
25 P. Debye and E. Hückel, *Phys. Z., 24* (1923) 185.
26 R. Szwarc, *J. Phys. Chem. Solids, 30* (1969) 705–711.
27 R.A. Young, *J. Nucl. Mater., 87* (1979) 283–296.
28 E.J. Yoffa and D. Adler, *Phys. Rev. B, 20*(10) (1979) 4044.
29 R. Fowler and E.A. Guggenheim, *Statistical Thermodynamics*, Cambridge University Press, Cambridge, 1965, p. 407.
30 G.S. Rushbrooke, *Trans. Faraday Soc., 36* (1940) 1055.
31 L.W. Barr and A.B. Lidiard, *Physical Chemistry – An Advanced Treatise*, Vol. X, Academic Press, New York, 1970, p. 51.